ACS OMEGA

http://pubs.acs.org/journal/acsodf

Article

Mechanistic Study of Diketopiperazine Formation during Solid-Phase Peptide Synthesis of Tirzepatide

Jingyao Wang,* Mark R. Berglund, Timothy Braden, Matthew C. Embry, Martin D. Johnson, Stephen R. Groskreutz, Fareed Bhasha Sayyed, Sergey Vladimirovich Tsukanov, Timothy D. White, Ankur Jalan, Kevin D. Seibert, and Michael E. Kopach*

Cite This: *ACS Omega* 2022, 7, 46809−46824

Read Online

ACCESS | Metrics & More | Article Recommendations | Supporting Information

ABSTRACT: This study focused on investigating diketopiperazine (DKP) and the formation of associated double-amino-acid deletion impurities during linear solid-phase peptide synthesis (SPPS) of tirzepatide (TZP). We identified that the DKP formation primarily occurred during the Fmoc-deprotection reaction and post-coupling aging of the unstable Fmoc-Pro-Pro-Ser-resin active pharmaceutical ingredient (API) intermediate. Similar phenomena have also been observed for other TZP active pharmaceutical ingredient (API) intermediates that contain a penultimate proline amino acid, such as Fmoc-Ala-Pro-Pro-Pro-Ser-resin, Fmoc-Pro-Pro-Pro-Ser-resin, and Fmoc-Gly-Pro-Ser-Ser-Gly-Ala-Pro-Pro-Ser-resin, which are intermediates for both hybrid and linear synthesis approaches. During post-coupling aging, it is found that Fmoc deprotection can proceed in dimethylformamide (DMF), dimethyl sulfoxide (DMSO), *N*-methyl-2-pyrrolidone (NMP), and acetonitrile (ACN) solvents without any piperidine addition. Density functional theory (DFT) calculations showed that a peptide that has a penultimate proline stabilizes the transition state through the C−H···π interaction during Fmoc decomposition, which causes those peptides to be more prone to cascade-deprotection reactions. Pseudo-reaction pathways are then proposed, and a corresponding macrokinetics model is developed to allow accurate prediction of the TZP peptide intermediate self-deprotection and DKP formation rate. Based on those studies, control strategies for minimizing DKP formation were further investigated and an alternative to Fmoc protection was identified (Bsmoc-protected amino acids), which eliminated the formation of the DKP byproducts. In addition, the use of oxyma additives and lower storage temperature was demonstrated to markedly improve the peptide intermediate stability to DKP degradation pathways.

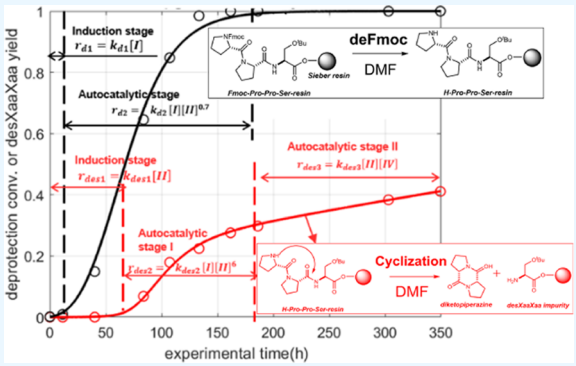

INTRODUCTION

Tirzepatide (TZP), a 39-amino-acid synthetic peptide, is a once-weekly novel glucose-dependent insulinotropic polypeptide (GIP) and glucagon-like-peptide-1 (GLP-1) receptor agonist. TZP, branded as Mounjanro, has been approved in the U.S. for blood glucose management in adults with type 2 diabetes and is currently in development for chronic weight management, non-alcoholic steatohepatitis (NASH), and other important indications at Eli Lilly and Company. The TZP sequence consists of a 39-amino-acid peptide backbone containing the noncoded amino acid aminoisobutyric acid (Aib) in two positions, a C-terminus amide, and a C20 fatty acid covalently attached at lysine 20 through a linker (Figure 1).

TZP is a synthetic peptide that has two primary routes of synthesis, a stepwise build-out by linear synthesis and a hybrid solid-phase peptide synthesis (SPPS)/liquid-phase peptide synthesis (LPPS) approach.[1,2] A key region of concern in either approach is the triproline region near the C-terminus, where it is essential to control the formation of double deletion impurities arising from 2,5-diketopiperizine (DKP) side reactions. Uncontrolled side reactions may pose a significant quality risk for pharmaceutical active pharmaceutical ingredient (API) syntheses, as well as a substantial downstream purification burden. This work focuses on the 2,5-diketopiperazine (DKP) formation side reactions observed during SPPS of TZP (Figure 1) and API intermediate fragment 1 (Figure 2) in use for a hybrid synthesis. DKP formation is known as one of the most challenging side reactions in peptide syntheses and it can potentially occur during both SPPS and extended peptide storage. For C to N peptide elongations, DKP processes are known to occur to the residue immediately after α-proline. This reaction is shown in Figure 3 and involves nucleophilic

Received: September 12, 2022
Accepted: November 21, 2022
Published: December 6, 2022

https://doi.org/10.1021/acsomega.2c05915
ACS Omega 2022, 7, 46809−46824

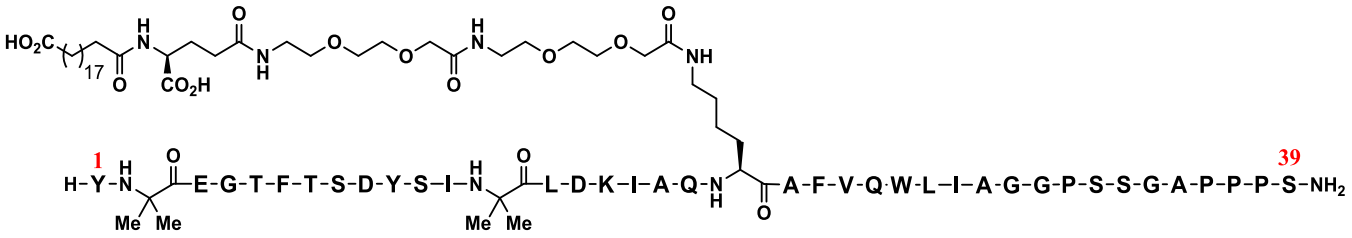

Figure 1. TZP Sequence.

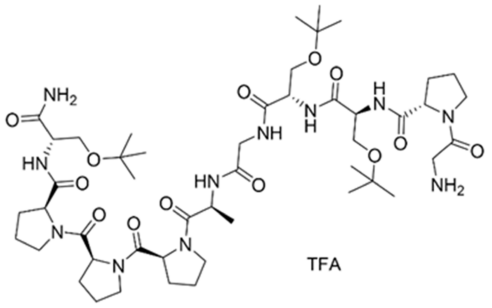

Figure 2. TZP fragment 1 molecular structure.

attack of the N-terminal nitrogen on the amide carbonyl between the second and third amino acids, which cleaves those two amino acids, yielding desXaaXaa impurity and forming a DKP byproduct.

Extensive past research has focused on identifying the root cause of DKP formation. The undesired DKP side reactions during SPPS have been found to be particularly problematic with certain peptide sequences[3−5] and benzyl-type peptide resin linkages[4,6] and catalyzed by acidic or basic conditions.[4,7,8] Rydon and Smith found that DKP formation is peptide sequence dependent and occurs more readily if proline or glycine residues are at position 1 or 2.[9,10] More interestingly, glycylproline (Gly-Pro) is much more readily formed than prolylglycine (Pro-Gly). They concluded it was because the Gly-Pro sequence has a favorable conformation of the side chain and a greater degree of fixation of the atoms in the Gly-Pro peptide ester.[9] In addition to Pro-Gly and Gly-Pro, Gisin and Merrifield and others also found that sequences such as Val-Pro, Pro-Pro, and Ala-Pro are more sensitive to the formation of DKPs.[11] Pederoso et al. observed DKP formation during SPPS with Fmoc amino acids and p-alkoxybenzyl ester resin, where piperidine is a very efficient catalyst.[12]

Methods have been developed to inhibit DKP side reaction propagation.[4,5,13−15] DKP formation can be avoided or minimized by utilizing mild deprotection conditions or incorporating a dipeptide to skip DKP-sensitive intermediates.[16] Goolcharran and Borchardt studied the impact of pH, temperature, and buffer concentration/species on the Phe-Pro-*p*-nitroaniline (Phe-Pro-pNA) to Phe-Pro-diketopiperazine (Phe-Pro-DKP) reaction.[17] They found that the DKP reaction followed pseudo-first-order kinetics with significant dependence on pH. Phe-Pro-DKP was found stable in the pH range of 3−8, while it underwent hydrolysis to the dipeptide under acidic and basic conditions outside the pH 3−8 range. Sun et al. reported a one-step method for the synthesis of DKP using an Fmoc-protected amino acid and an amino acid ester in the presence of 2-(2,5-dioxopyrrolidin-1-yl)-1,1,3,3-tetramethylisouronium tetrafluoroborateo-(*n*-succinimidyl)-1,1,3,3-tetramethyluronium tetrafluoroborate (TSTU) and triethanolamine (TEA) in DMF at 50 °C, indicating that even Fmoc-protected peptides can be susceptible to DKP formation under strongly basic conditions.[13] Suzuki et al. proposed the use of HCl in dioxane as a deprotection reagent for SPPS with Boc/Bzl-protecting group strategy, which successfully suppresses the DKP formation.[14] Alternatively, Gairl et al. investigated the use of the benzotriazol-1-yloxytris(dimethylamino)phosphonium hexafluorophosphate (BOP) coupling reagent with *N*,*N*-diisopropylethylamine (DIPEA), which substantially inhibited the DKP formation during SPPS coupling of a third amino acid to dipeptides on a nitro-benzylic resin linker.[4] Pawlas et al. investigated DKP formation during the Fmoc deprotection of Fmoc-Arg(Obf)-Leu-Cam resin. A significant quantity of DKP was identified only 8 min into the 20% piperidine deprotection at room temperature. They demonstrated that utilizing a lower piperidine concentration and temperature for the Fmoc deprotection suppressed DKP formation.[5]

SPPS is the main methodology in use for the manufacture of synthetic peptides (Figure 4). High levels of the desProPro impurity were observed for some batches during linear SPPS of TZP, but specific conditions/factors leading to this byproduct in specific lots/experiments were not initially apparent. A typical desPro37Pro38 impurity build-up during TZP fragment 1 SPPS is presented in Figure 5. As it can be seen, the desProPro impurity is measurable at a significant level during the Fmoc-Pro36 (structure shown in Figure 6) and Fmoc-Ala 35 (structure shown in Figure 6) coupling reactions stage.

In this work, we identified novel self-deprotection side reactions of Fmoc-protected peptide intermediates under various solvent and temperature conditions. This was found to be a major causal factor for DKP formation in the systems studied. A detailed reaction mechanism for the deFmoc reaction is proposed via density functional theory (DFT) calculations. Then, a macrokinetics model is built to predict

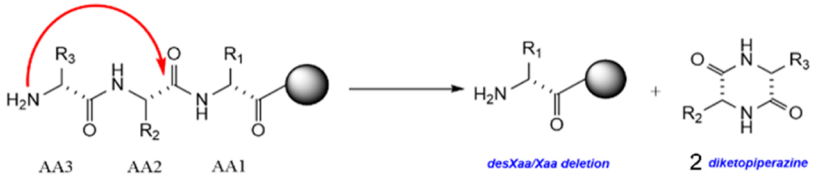

Figure 3. DKP formation mechanism.

https://doi.org/10.1021/acsomega.2c05915
ACS Omega 2022, 7, 46809−46824

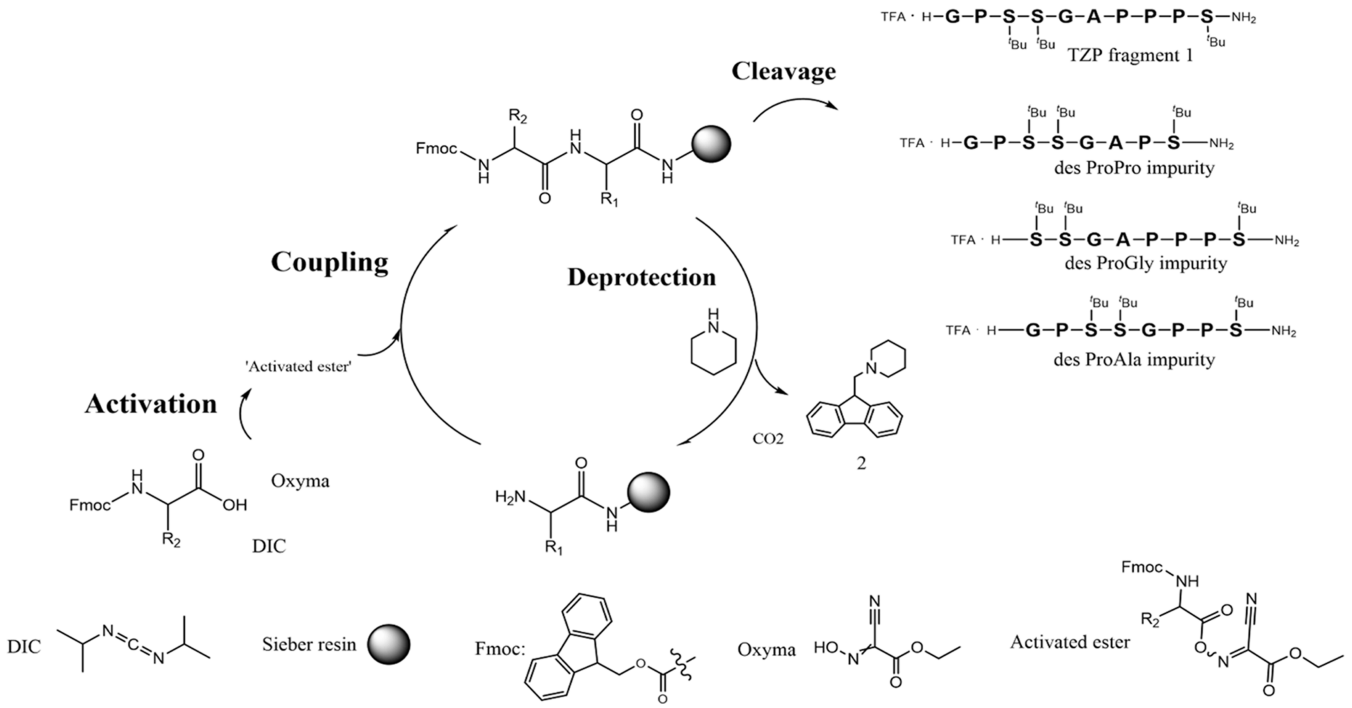

Figure 4. Solid-phase peptide synthesis framework and associated desXaaXaa impurity formation.

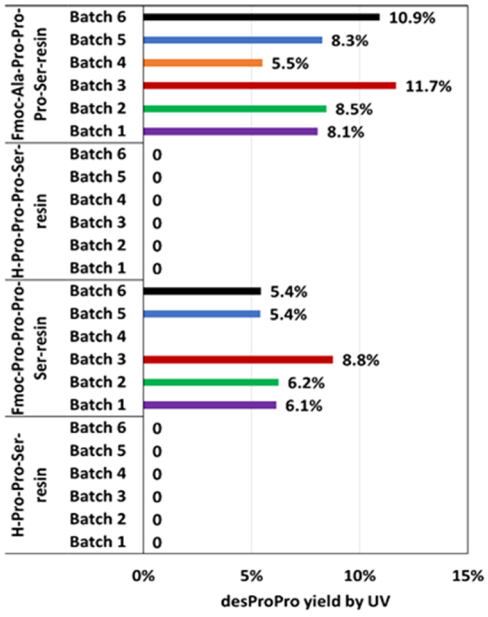

Figure 5. desProPro formation during TZP fragment 1 synthesis.

the rate of deFmoc and DKF formation. The conditions for minimizing DKP impurities are finally proposed, which eventually allow to control the desProPro impurity below 0.5% in TZP fragment 1 synthesis.

RESULTS AND DISCUSSION

Impurity Root Cause Analysis. We conducted desProPro root-cause analysis by summarizing the SPPS parameters and the corresponding desProPro level for multiple batches. Then, a single-factor analysis was performed (results shown in Supporting Information in Figure S1) based on 6 batches of TZP Fragment 1 synthesis parameters described in the Experimental Section Synthesis condition of TZP API intermediates. From the single-factor analysis, we found that several factors are positively correlated with the desProPro yield, which includes residual piperidine concentration after deprotection wash, amino acid/oxyma/DIC age in the DMF solvent, the TZP API intermediate Fmoc-Pro37 (structure shown in Figure 6) hold time, and Fmoc-Pro37 deprotection time.

Based on this data analysis, we proposed major hypotheses for the desProPro formation: (i) desProPro formed during the Fmoc-Pro-Pro-Ser-resin deprotection reaction; (ii) desProPro formed during the hold time of Fmoc-Pro-Pro-Ser-resin after DMF wash; and (iii) desProPro was formed during the coupling of Fmoc-Pro-OH to H-Pro-Ser-resin due to the long hold time for the activation reagent feed and high residual piperidine concentration. According to the literature survey, hypothesis (i) has been verified multiple times and it has been found that a proline-containing peptide can form DKP under piperidine basic conditions.[5,17] However, for hypotheses (ii) and (iii), where the Fmoc group is still protecting the peptide, there is little indication in the literature that the DKP side reaction would occur. For this reason, controlled experiments have been conducted and the results will be discussed in the following sections.

DKP Formation during the Deprotection Reaction with Piperidine. According to desProPro formation single-factor analysis, we found that the desProPro formed is correlated with deprotection time and piperidine concentration. For this reason, the next hypothesis focused on desProPro formation during the Fmoc-Pro37 deprotection reaction. Six controlled experiments were conducted, and the results are listed in the Supporting Information Table S1 and Figure S2. As shown in Table S1, the impacts of mixing, piperidine charge volume, concentration, and stoichiometric ratio of piperidine over the active resin site on the desProPro formation are evaluated on the DKP impurity during the deprotection reaction. The kinetics data of desProPro formation were taken periodically

https://doi.org/10.1021/acsomega.2c05915
ACS Omega 2022, 7, 46809−46824

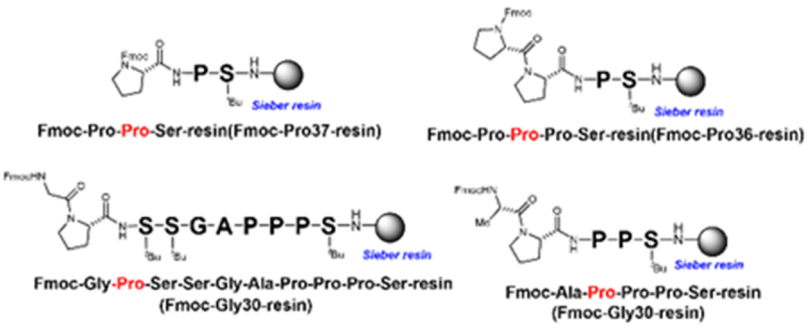

Figure 6. TZP API intermediates subject to desXaaXaa formation.

Table 1. Controlled Experiments for Testing DKP Formation during the Coupling Reaction to Produce Fmoc-Pro-Pro-Pro-Ser-Resin

entry	Fmoc-Pro-Pro-Ser-resin starting material hold time (h)	20% PIP added (μL)	proline/oxyma/DIC solution age (h)	coupling time (h)	activated ester eq.	desProPro (%) by UV
1	48	0	6	1	2.5	14.8
2		0	1800	1	2.5	14.7
3		100	6	1	2.5	15.3
4	2	0	6	1	2.5	0.7
5		0	6	18	2.5	0.5
6		0	6	1	1000	0.6

and analyzed using liquid chromatography−mass spectrometry (LC−MS) for 24 h. We found that desProPro formation is more significant without mixing, implying that impurity formation is potentially more severe under storage conditions. The reaction kinetics follows a pseudo-zero-order reaction mechanism. The DesProPro formation rate varies in the range of 0.2 to 0.4%/h depending on the exact conditions. These findings clearly indicate significant desProPro formation, i.e., long deprotection time during Fmoc-Pro-Pro-Ser-resin deprotection would significantly increase the desProPro formation. With this knowledge, we conducted a new experiment, applying two stirs of 5 volumes of 20% piperidine (1st stir 16 min, 2nd stir 87.3 min) for the Fmoc-Pro37 deprotection reaction, and only 1.3% desProPro was formed.

DKP (Compound 1 in Figure 3) and Dibenzofulvene (DBF)-piperidine (Compound 2 in Figure 4) and are the two key byproducts of the Fmoc-deprotection reaction and the DKP impurity formation reaction, respectively. We proposed two hypotheses on the impact of side products on the DKP formation rate: (i) catalyzing the effects of DBF-piperidine and (ii) catalyzing the effects from DKP. To further verify these hypotheses, three controlled experiments were conducted and desProPro formation kinetics were measured periodically over 140 hours (see the Supporting Information Table S2 and Figure S3).

As it can be seen, DBF-piperidine does not show a catalyzing effect on the DKP formation compared to the baseline condition in the DMF solvent. DKP, on the other hand, significantly increased the desProPro formation rate. As DKP is a byproduct of desProPro formation, it indicates that the reaction is inherently autocatalytic or exhibits the properties of a cascade reaction. Past studies have shown that DKP formation is catalyzed by basic conditions.[8,11,17] CO_2 is also a byproduct of the Fmoc-deprotection reaction, which can build up in solution, potentially buffering the solution to be less basic. Further studies can be conducted to understand any impact the CO_2 concentration may have on DKP formation.

DKP Formation during the Coupling Reaction. According to desProPro formation single-factor analysis, we found that amino acid/oxyma/DIC age in the DMF solution, Fmoc-Pro-Pro-Ser-resin API intermediate hold time in DMF, and residual piperidine level before coupling are positively correlated with desProPro impurity level. For this reason, we focused on investigating those factors as potential root causes of desProPro impurity formation. We conducted six controlled experiments to test those variables as listed in Table 1. For all controlled experiments, two lots of Fmoc-Pro-Pro-Ser-resin API intermediate, with 48 and 2 h room temperature hold time, respectively, were chosen as starting materials. Those materials were treated with 9 volumes of 20 vol % piperidine in DMF and deprotected for 50 min. Prior to the coupling reaction, LC−MS analysis was conducted verifying 100% deprotection conversion. Then, for all entries 1−6, the activation reaction was stirred for 30 min. In the first three entries with 48 h starting material hold time, we observed that 14.8 to 15.3% desProPro was formed despite different coupling conditions. This indicates that the Fmoc-Pro-Pro-Ser-resin intermediate already contained ≈15% desProPro impurity before the coupling reaction. Further LC−MS analysis confirmed that the Fmoc-Pro-Pro-Ser-resin intermediate was fully deprotected by the end of the 48 h hold time.

For entries 4−6 with a 2 h hold time in Table 1, we found that less than 1% of desProPro formed under various coupling reaction conditions. Further analysis showed that no single proline deletion impurity was found for all entries 1−6, indicating that double amino acid deletion did not occur (if double prolines were deleted, the resulting desProPro peptide would couple with proline, generating a single proline deletion impurity). Those experiments further confirmed that desProPro was not formed during the coupling reaction, but instead was formed before the coupling reaction started.

DKP Formation during the Post-Coupling Hold Time. We further extended the Fmoc-Pro-Pro-Ser-resin API intermediate hold time up to 96 h in DMF to understand the stability. We measured the self-deprotection rate and subsequent DKP

https://doi.org/10.1021/acsomega.2c05915
ACS Omega 2022, 7, 46809−46824

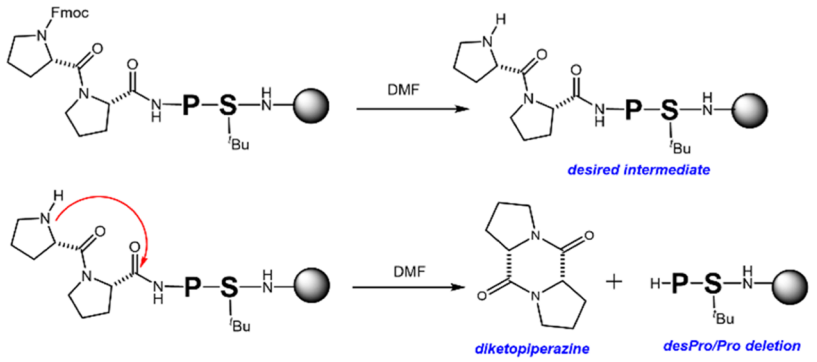

Figure 7. Fmoc-Pro-Pro-Ser-resin self-deprotection and DKP formation.

Table 2. Past Self-Deprotection Occurrences of TZP API Instability during Storage

TZP API intermediate and model peptide nomenclature	storage temp (°C)	storage time (days)	sample status	deprotection conversion (%)
Fmoc-Ala-Pro-Pro-Pro-Ser-resin	3	242	wet	82
Fmoc-Ala-Pro-Pro-Pro-Ser-resin	−20	243	dry	8
Fmoc-Gly-Pro-Ser-Ser-Gly-Ala-Pro-Pro-Ser-resin	−20	410	dry	49
Fmoc-Pro-Ser-Ser-Gly-Ala-Pro-Pro-Ser-resin	3	238	dry	1

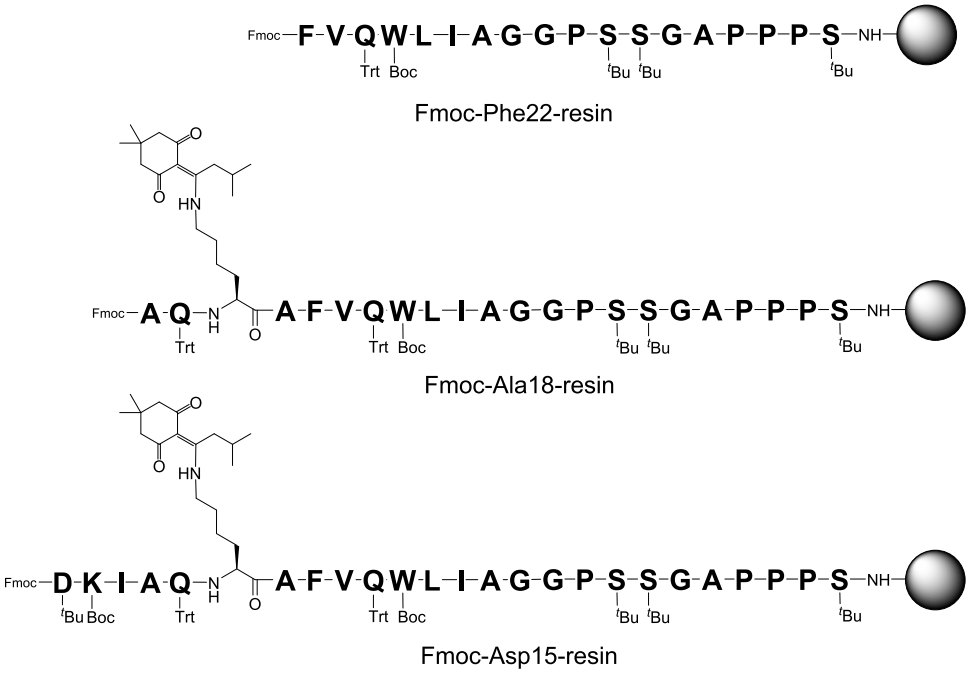

Figure 8. TZP API intermediates investigated to be found with minimal potential for desXaaXaa formation.

formation kinetics for DMF-wetted Fmoc-Pro-Pro-Ser-resin (solvent amount 15 g DMF/g resin). The results are shown in Supporting Information Figure S4, which show that both self-deprotection and desProPro formation rates are sufficiently fast. Further NMR analysis of the DMF solution shows that the weight percent DKP was ∼1.55% (relative to the total mass of DMF and DBF in the solution phase). Also, the DBF was measured to be ∼2.39 molar equivalents (relative to DKP), which further confirms the API instability in DMF due to self-deprotection and DKP formation.

Those findings indicate that Fmoc-Pro-Pro-Ser-resin can go through a self-deprotection reaction and subsequent DKP formation in DMF without any added base as indicated in Figure 7. As shown in Table 2, past TZP API intermediates were analyzed and various deprotection conversions are found in Table 2. To our knowledge, the self-deprotection reaction has not been reported in the literature, nor in previous syntheses at Lilly, and it tends to go unnoticed since the following step is FMOC removal (Figure 8).

We found that the desProPro impurity from the DKP side reaction was not formed during Fmoc-Pro-Pro-Pro-Ser-resin coupling. Peptide intermediates are stable with old AA/oxyma/DIC solutions, high equivalent of coupling solutions relative to active sites, and long activation times. Even residual piperidine in the resin does not cause desXaaXaa impurity during the coupling reaction. The desProPro impurity is actually formed during the post-coupling hold time of Fmoc-Pro-Pro-Pro-Ser-resin due to self-deprotection and subsequent DKP formation. We found that peptides are particularly vulnerable to this instability when proline is the penultimate

https://doi.org/10.1021/acsomega.2c05915
ACS Omega 2022, 7, 46809−46824

amino acid. We found an autocatalytic behavior of desProPro formation where the DKP byproduct promotes the formation of more desProPro.

Reaction Mechanism Study for DKP Formation. *Impact of Peptide Sequence.* We measured the stability kinetics data for other TZP API intermediates on Sieber resin (Figure 6) in DMF under room temperature and the results are shown in Supporting information in Figure S5. It was found that all of the peptides tested are unstable in DMF; however, Fmoc-Pro37-resin is the least stable and desProPro formation can reach up to 80% after 650 h. On the other hand, desXaaXaa formation for Fmoc-Ala35-resin, Fmoc-Pro36-resin, and Fmoc-Gly30-resin reached levels of 15, 25, and 5%, respectively. It is observed that each of these four API intermediates has proline as the penultimate amino acid (Figure 6). This was also confirmed with other peptide stability experiments of TZP that are listed in Supporting Information in Table S3.

We further synthesized five trimer model peptides as shown in Figure 9 to test our hypothesis. The results in Table 3 and

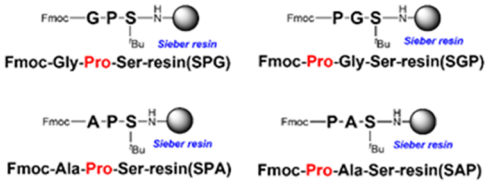

Figure 9. Structure of four trimer model peptides.

Figure 10 show that, compared with peptides with penultimate proline, peptides with terminal proline undergo much slower self-deprotection and there is no formation of desXaaXaa. The results further confirm that self-deprotection and desXaaXaa formation become more likely if the peptide contains a penultimate proline. The rate of self-deprotection and following DKP formation is most significant for the Fmoc-Pro-Pro-Ser-resin intermediate. This is in agreement with the literature report that DKP formation is particularly problematic when a sterically unhindered amino acid such as glycine is followed by an amino acid more likely to adopt cis-amidite conformations of L- and D-amino acids.[18−20]

Impact of Solvent. The stability of Fmoc-protected TZP API intermediates on resin—Fmoc-Ala35-resin, Fmoc-Pro-Pro-Ser-resin, and Fmoc-Gly-Pro-Ser-resin—was tested in different solvents at 20 °C. DMF, NMP, DMSO, and ACN were selected for the study. The experimental conditions are summarized in Supporting Information Table S3. The stability of SPP, SPPPA, and SPG in different solvents is presented in Figures S6−S8, respectively. It is found that for all peptides the self-deprotection rate proceeds the quickest in DMSO followed by DMF and then NMP, with the self-deprotection being the slowest in ACN. Comparing the desXaaXaa formation rates, for all peptides the desXaaXaa formation rate is the fastest in NMP or DMF, with DMSO and acetonitrile being slower. These results show two important observations: (i) self-deprotection and desXaaXaa formation are strongly dependent on the pK_a and/or polarity of the solvent; (ii) mass transfer limitation may also affect the rate of peptide instability, as Sieber resin does not swell sufficiently in acetonitrile. Also, dry resin was found to be more stable than wet resin during storage.

Impact of Protecting Groups. The Fmoc protecting group is a very nonpolar functional group, which imparts poor solubility in a polar aprotic solvent such as DMF. To address the concern that this solubility mismatch may be promoting the deprotection of the terminal AA, utilization of the Bsmoc-protecting group was evaluated for comparison. The Bsmoc-protecting group can be used interchangeably with the analogous Fmoc species as they can be removed under similar basic conditions using piperidine. Coin et al. found that application of the Bsmoc-protecting group can significantly suppress the diketopiperazine formation.[21,22] In fact, it provides an advantage over the Fmoc model because the resulting byproduct is always an adduct of piperidine, which is very soluble and easily washed from the resin. Conversely, Fmoc often generates an appreciable level of dibenzofulvene (DBF), which is poorly soluble and prone to polymerization. Structurally, the Bsmoc-protecting group contains a sulfone moiety, which makes it significantly more polar (esp. relative to Fmoc), hypothetically making it a much better match with the polar nature of DMF.

To evaluate this hypothesis, we compared the stabilities of Fmoc- and Bsmoc-protected Gly-Pro-Ser peptides (Figure 11) in DMF at 20 °C, and the results are shown in Supporting Information Figure S9. It is found that the Bsmoc-protected peptide has a much slower self-deprotection rate than the Fmoc-protected peptide and desProGly impurity is not detected. This finding indicates that (i) self-deprotection and desXaaXaa formation are not triggered by the dimethyl amine impurity in DMF since both Bsmoc- and Fmoc-protecting groups can be removed via the base DMF solvent, which is of high purity, as confirmed by the NMR analysis shown in the Supporting Information in Figure S12; (ii) the Bsmoc group is more stable than the Fmoc group for peptides with a penultimate proline in the DMF solvent. These results are also in line with past literature findings.[21,22]

Although the Bsmoc-protecting group demonstrated astonishingly better stability in this example, Bsmoc-protected amino acids are not commonly available for use in SPPS. Therefore, these reagents are not competitively priced, and their use should be reserved for builds that show high levels of impurities (DKP formation, addition impurities, etc.). Likely as more alternatives to the Fmoc-protecting group are adopted in

Table 3. Stability Comparison of Trimers (All Experiments Were Conducted at Room Temperature in DMF with 15.67 g Solvent/g Resin Amount)

peptide structure	nomenclature	time to reach 50% self-deprotection conversion (h)	desXaaXaa (%)
Fmoc-Pro-Pro-Ser(^{t}Bu)-resin	SPP	13	73
Fmoc-Ala-Pro-Ser(^{t}Bu)-resin	SPA	66	37
Fmoc-Pro-Ala-Ser(^{t}Bu)-resin	SAP	175	0
Fmoc-Gly-Pro-Ser(^{t}Bu)-resin	SPG	70	41
Fmoc-Pro-Gly-Ser(^{t}Bu)-resin	SGP	275	0

https://doi.org/10.1021/acsomega.2c05915
ACS Omega 2022, 7, 46809−46824

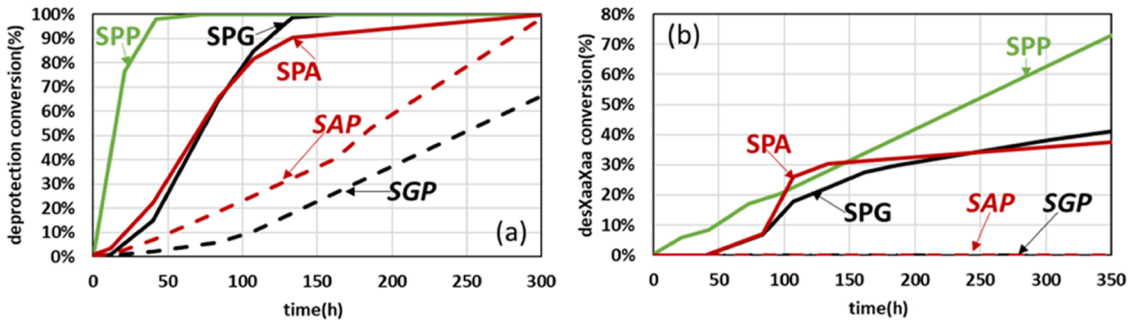

Figure 10. Comparison of trimer stability with proline as the penultimate and ultimate amino acid: (a) deprotection conversion and (b) desXaaXaa formation.

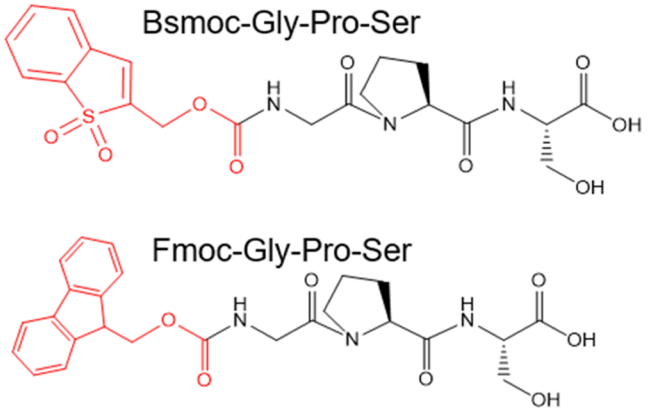

Figure 11. Formula for Bsmoc- and Fmoc-protected peptides.

industrial applications, the pricing differences will become less substantial (Figure 12).

Impact of Oxyma Additives. Addition of oxyma will increase the acidity of the solvent and for this reason, we tested the impact of oxyma additives on Fmoc-Pro37 stability in terms of self-deprotection in DMF. The experimental conditions and results are listed in Table S5 and Figure S10. As can be seen, even 0.2 wt % of oxyma will significantly stabilize the peptide. This further confirms that peptide instability is strongly impacted by the pH of the solution phase.

Impact of Temperature. We measured the Fmoc-Ala-Pro-Pro-Pro-Ser-Resin peptide instability under different temperatures, and the conditions and results are shown in Supporting Information Table S6 and Figure S11. It is found that Fmoc-Ala-Pro-Pro-Pro-Ser-Resin is stable at −22 °C and suitable for long-term storage, while 3 °C can be used for shorter hold times.

Molecular Simulations of Fmoc Self-Deprotection Mechanisms. To unravel the origin of Fmoc group decomposition and the effect of penultimate proline amino acid on the stability, we performed density functional theory (DFT) calculations on two systems, namely SAP (Fmoc-Pro-Ala-Ser) and SPP (Fmoc-Pro-Pro-Ser). SPP represents a system that has proline present at the penultimate position and SAP represents a system wherein proline is not at the penultimate position. Experimentally, it is observed that SPP shows Fmoc decomposition (deprotection conversion 60% at

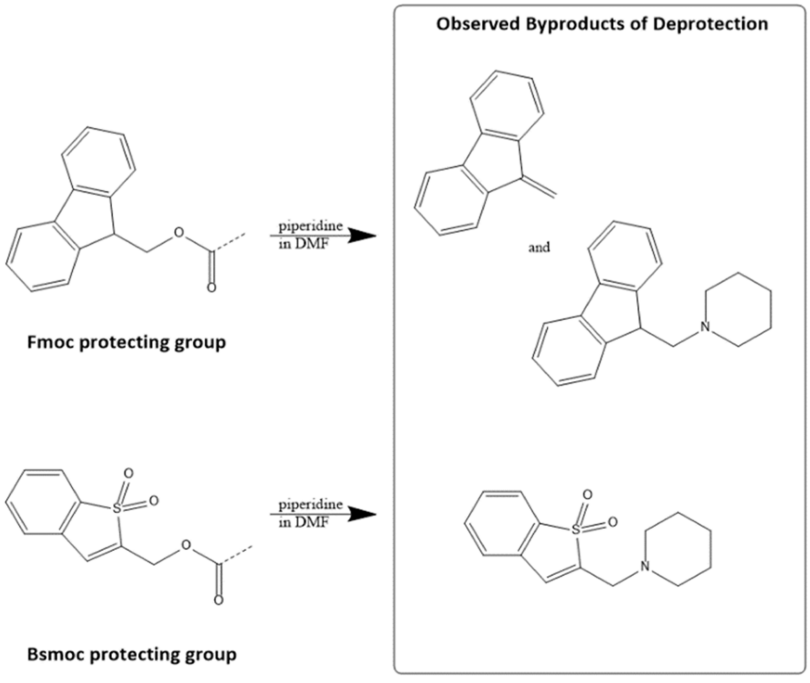

Figure 12. Fmoc and Bsmoc deprotection and its byproduct.

https://doi.org/10.1021/acsomega.2c05915
ACS Omega 2022, 7, 46809−46824

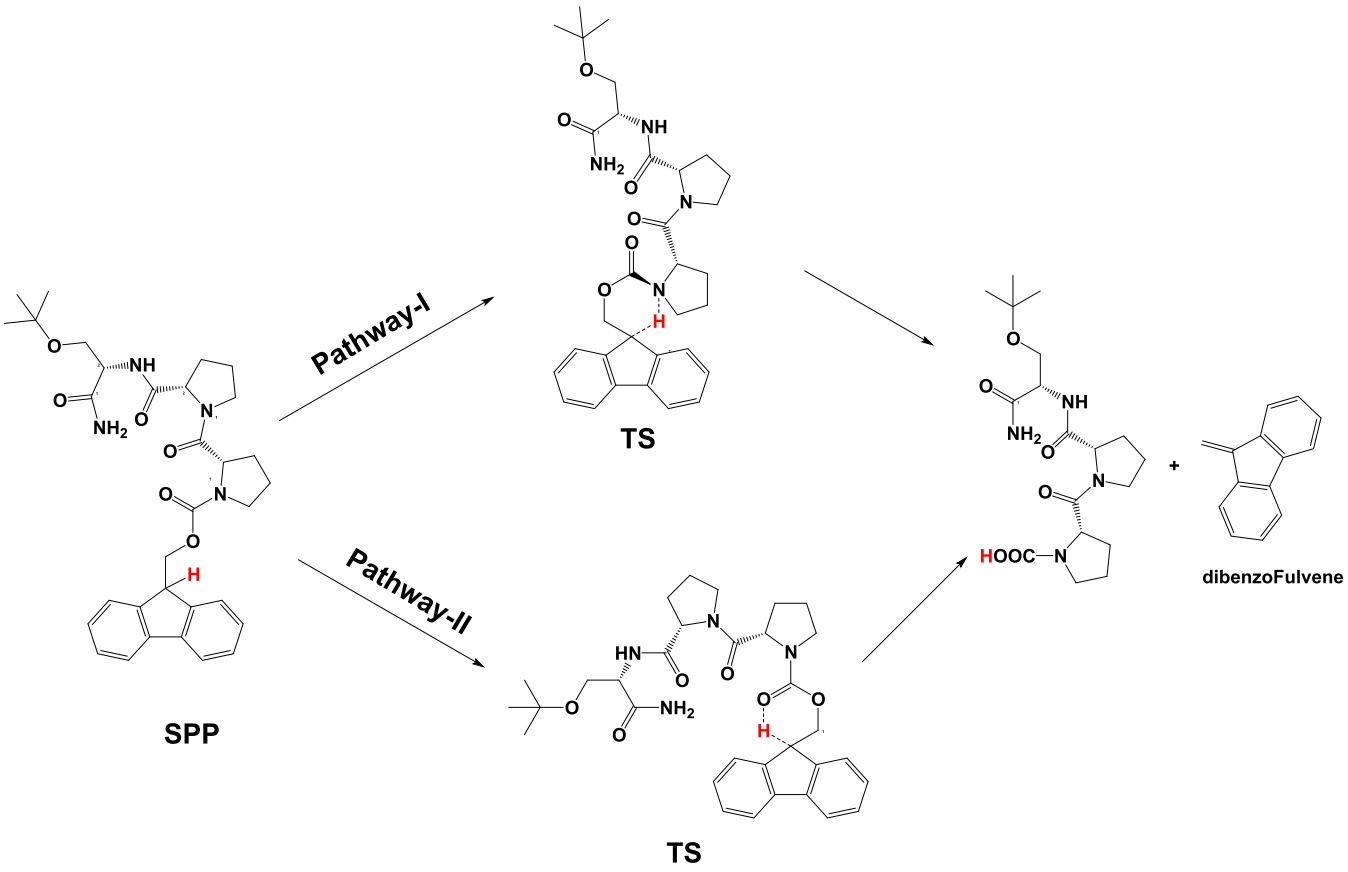

Figure 13. Fmoc decomposition pathways. An example is shown for the SPP molecule.

24 h) whereas SAP does not (deprotection conversion 0% at 24 h).

In Figure 13, two probable mechanisms are considered for the Fmoc decomposition. Pathway-I proceeds through the abstraction of 9H of the Fmoc group (marked in red color) by the N-atom of proline via a six-membered transition state.

Pathway-I: C−H Activation by the N-Attack of Proline. In Figure 14, the Gibbs free energy profile for the SPP and SAP decomposition via pathway-I is shown. The Gibbs activation energy ($\Delta G^{\ddagger}$) for the SPP decomposition is 40.6 kcal/mol, whereas the $\Delta G^{\ddagger}$ for the SAP decomposition is 47.6 kcal/mol. The trend in $\Delta G^{\ddagger}$ indicates that SPP decomposition is easier when compared with the SAP. To understand the reasons for the lower $\Delta G^{\ddagger}$ shown by the SPP when compared to SAP, optimized TS geometries are examined.

In Figure 15, the transition states involved in the SPP and SAP decomposition are shown. The C−H bond of 9H FMOC increased from 1.098 to 1.584 and 1.588 Å for SPP and SAP, respectively. Similarly, the N−H bond distance is 1.177 and 1.159 Å for SPP and SAP, respectively, indicating that the transition state is close toward the products. In the case of SPP, the CH···π interaction observed for one of the C−H groups of proline pointed toward the π-cloud of the benzenoid ring of Fmoc. In CH···π interactions, the C−H bond is considered as a donor and π-system as an acceptor. In the case of SAP, no such strong CH···π interaction is present. Further, the distance between the H of the nearest C−H and centroid from the benzenoid ring of Fmoc also indicates the stabilization of TS in the SPP over the SAP. The C−H···π distance is 2.329 Å for the SPP and 3.052 for the SAP, and the near-linear angle suggests that C−H···π interaction[23] stabilizes the TS in SPP over the SAP, and hence the lower $\Delta G^{\ddagger}$. The dominant role of such C−H···π interactions was previously confirmed by Ganguly et al.[24] in the case of peptides with Pro-Pro motifs using NOESY experiments. Further, the presence of C−H···π interaction plays a significant role in the reaction chemistry as well.[25]

Pathway-II: C−H Activation by the O-Attack of the Carboxyl Group of Proline. In Figure 16, the Gibbs free energy profile for the SPP and SAP decomposition via pathway-II is shown. The $\Delta G^{\ddagger}$ for the SPP decomposition is 34.8 kcal/mol, whereas the $\Delta G^{\ddagger}$ for the SAP decomposition is 35.5 kcal/mol. The trend in $\Delta G^{\ddagger}$ indicates that SPP decomposition is easier when compared with the SAP and the $\Delta G^{\ddagger}$ value is smaller for pathway-II than for pathway-I. The trend in $\Delta G^{\ddagger}$ indicates that Fmoc decomposition is favorable via pathway-II. Interestingly, pathway-II is a stepwise mechanism wherein the 1st step occurs with Fmoc cleavage through the C−H abstraction and the 2nd step occurs through the O−H migration to the N−H group with subsequent cleavage of CO_2. Pathway-I is a concerted step wherein both dibenzofulvene and CO_2 elimination occur simultaneously, which is further confirmed from the IRC calculations.

In Figure 17, the transition states involved in the SPP and SAP decomposition via pathway-II are shown. The C−H bond of 9H Fmoc increased from 1.086 and 1.080 to 1.584 and 1.588 Å for SPP and SAP, respectively. In the case of SPP, a strong CH···π interaction is observed between the C−H of proline and the π-cloud of the benzenoid ring of Fmoc. The C−H···π distance is 2.640 Å and ∠C−H···π is 176°, whereas the C−H···π distance (nearest C−H from the centroid of the benzenoid ring of Fmoc) for SAP is 3.390 Å and ∠C−H···π is

https://doi.org/10.1021/acsomega.2c05915
ACS Omega 2022, 7, 46809−46824

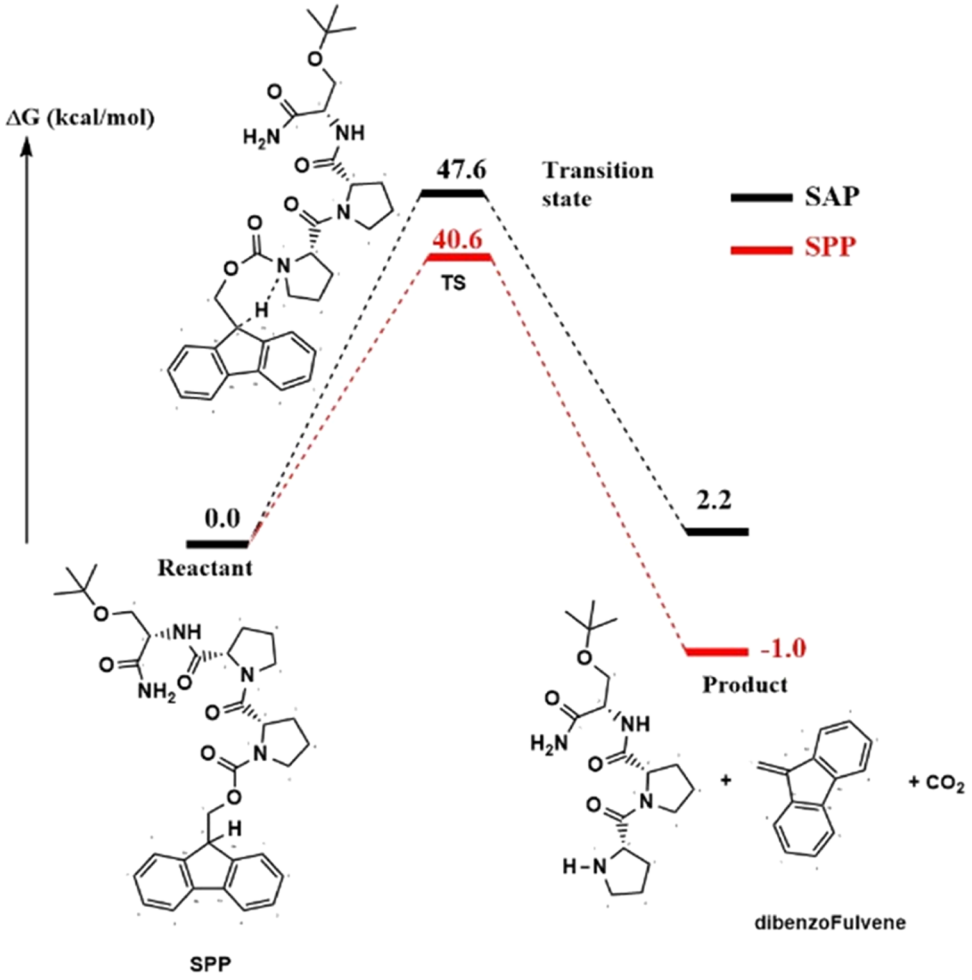

Figure 14. Gibbs free energy profile for the SPP and SAP decomposition via pathway-I. Black color represents SAP and red color represents SPP.

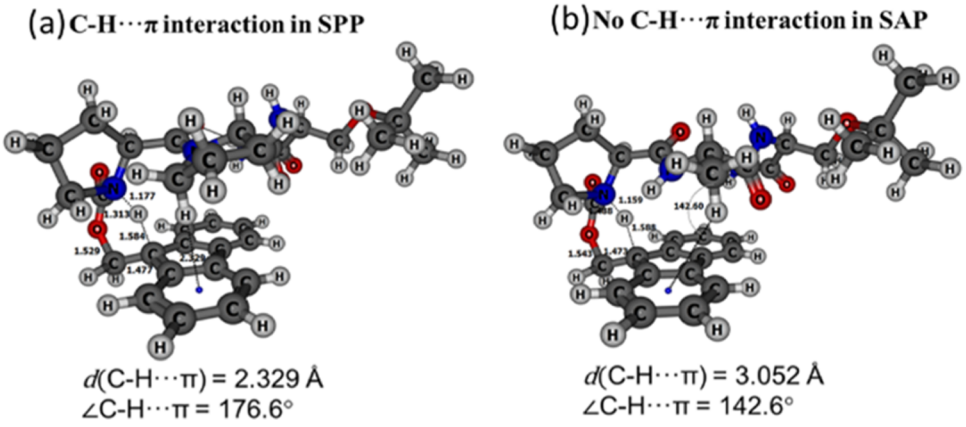

Figure 15. Transition-state geometries of SPP and SAP decomposition for pathway-I. d(C−H···π) is the bond distance between the H of C−H moiety and the center of the benzenoid ring of Fmoc. ∠C−H···π is the angle between C−H and the center of the benzenoid ring of Fmoc. (a) SPP (left); (b) SAP (right).

154.2°.[26] Similar to pathway-I, pathway-II also shows lower $\Delta G^{\ddagger}$ because of the presence of C−H···π interaction.

To further confirm the nature of the C−H···π interaction in SPP, we performed the noncovalent interactions (NCI) analysis developed by Yang and co-workers.[27] The regions of attractive and repulsive interactions can be identified through the generation of NCI plots. This analysis reveals a color-coded reduced-density gradient isosurface, in which regions corresponding to attractive interactions are colored as blue (strong) or green (weak), while repulsive regions are colored as red (strong). As shown in Figure 18, the large green area between the C−H of proline and the π-cloud of Fmoc shows the presence of C−H···π interaction in SPP.

In conclusion, the Fmoc decomposition occurs through a stepwise pathway-II mechanism wherein the carbonyl oxygen abstracts the C−H proton of Fmoc. The presence of the C−

https://doi.org/10.1021/acsomega.2c05915
ACS Omega 2022, 7, 46809−46824

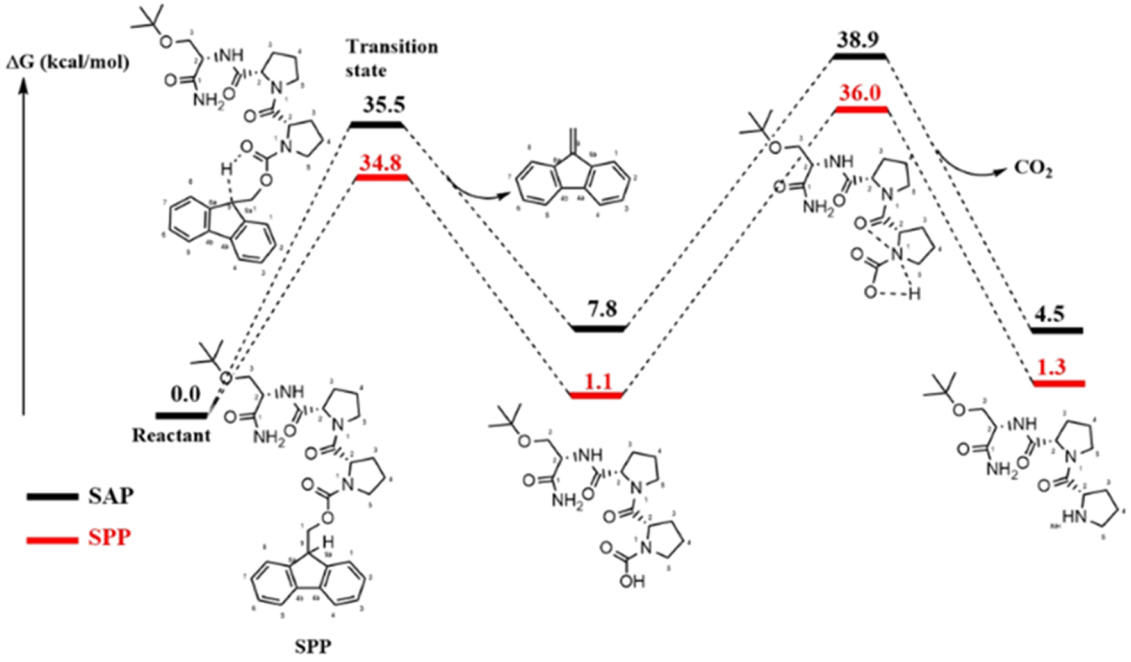

Figure 16. Gibbs free energy profile for the SPP and SAP decomposition via pathway-II. Black color represents SAP and red color represents SPP.

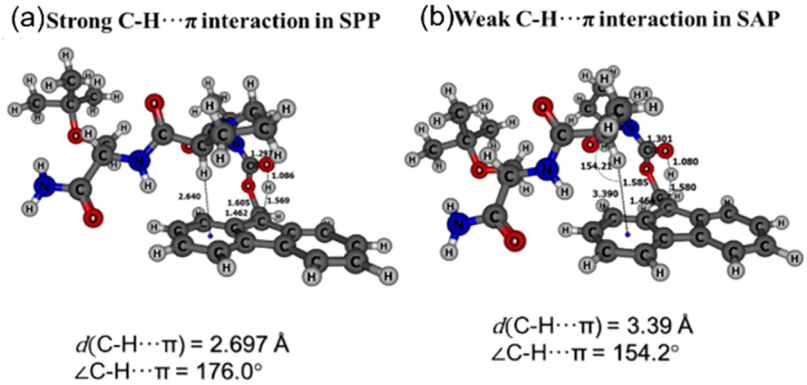

Figure 17. Transition-state geometries of SPP and SAP decomposition for pathway-II. d(C−H···π) is the bond distance between the H of C−H moiety and the center of the benzenoid ring of Fmoc. ∠C−H···π is the angle between C−H and the center of the benzenoid ring of Fmoc. (a) SPP (left); (b) SAP (right).

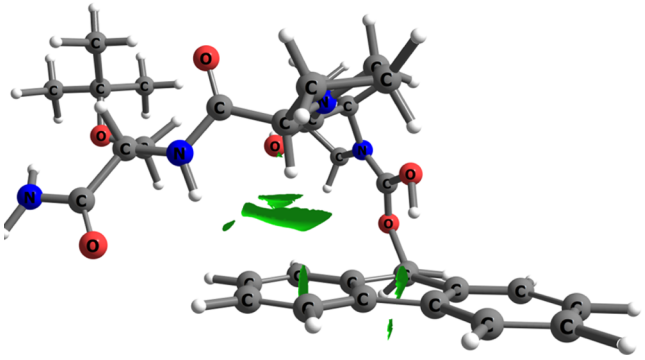

Figure 18. SPP: NCI plots showing the presence of C−H···π interactions between the C−H of proline moiety and the benzenoid ring of Fmoc.

H···π interaction in SPP, which has a penultimate proline, stabilizes the transition state during Fmoc decomposition and this is the reason why SPP has a lower $\Delta G^{\ddagger}$ compared to that of SAP.

Macro-Kinetics Modelling of Peptide Instability. A macrokinetics model was developed for the temperature range of −20 to 20 °C for different peptide sequences/solvent conditions to predict the rate of self-deprotection and subsequent DKP impurity formation.

Pseudo-Reaction Pathway. The purpose of the pseudo-reaction pathway is to propose suitable reaction rate equations to allow modelling of the complex experimental peptide degradation kinetics data presented in this work. For this reason, those pathways are not necessarily representative of the actual molecular interactions but are assumed to exist to explain the experimental observation evidence to allow fitting of parameters and hence accurately predict the rate of peptide degradation.[28−30] To propose the actual reaction pathway that occurs in the molecular level, a more rigorous and systematic molecular simulation/isotope labelling approach must be employed, which could be part of future work.[31,32] With those assumptions in mind, the proposed pseudo-reaction pathways that describe peptide self-deprotection are presented in Figure 19. The pathways include two independent routes:

https://doi.org/10.1021/acsomega.2c05915
ACS Omega 2022, 7, 46809−46824

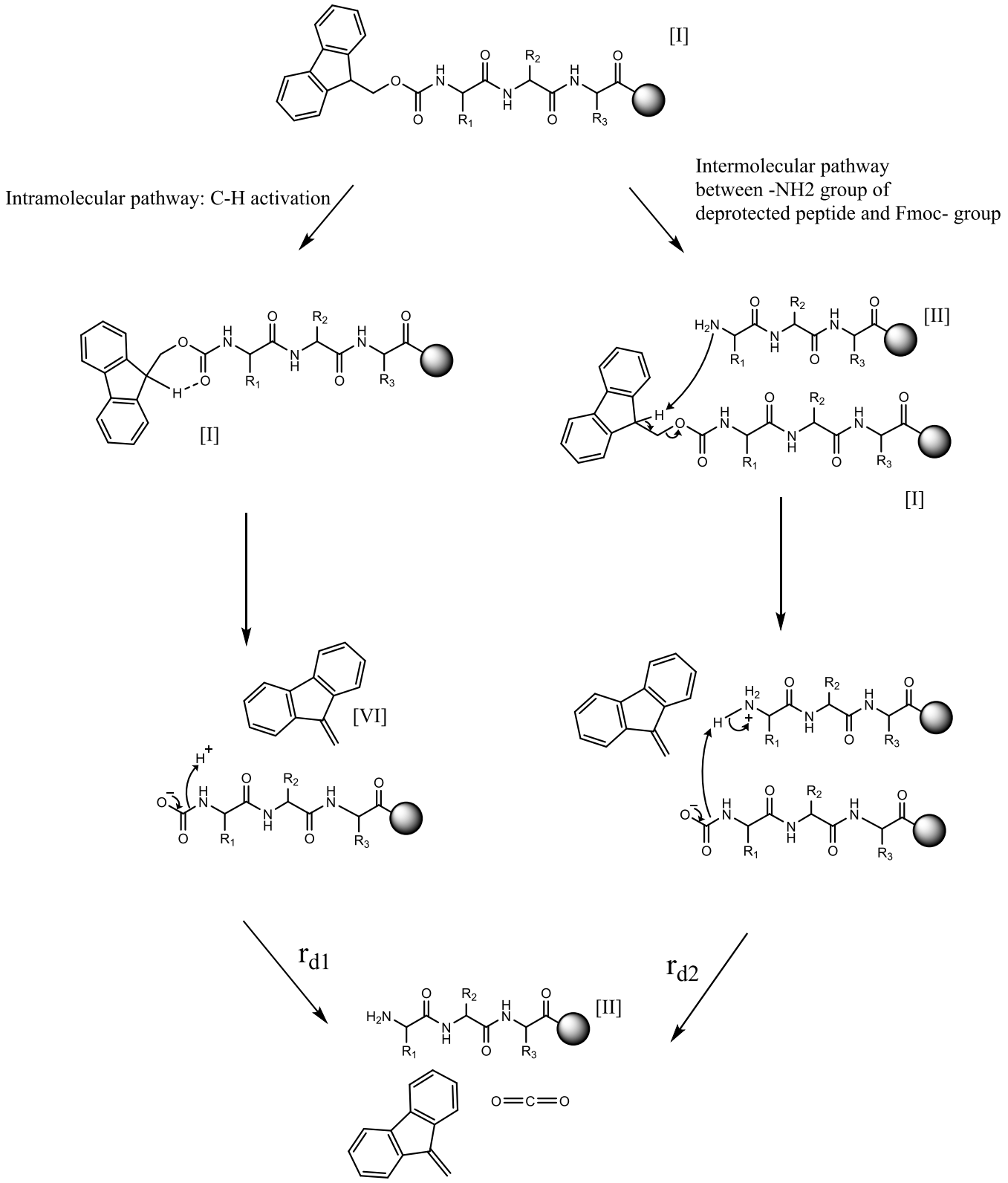

Figure 19. Pseudo-reaction pathways for the self-deprotection mechanism of the FMOC-protected peptide.

(i) the intramolecular pathway from C−H activation proposed from molecular simulation (r_{d1}); (ii) intermolecular pathways between the amine group of the deprotected peptide and the Fmoc group of the protected peptides (r_{d2}). The intramolecular pathway (i) is particularly significant when proline is the penultimate amino acid due to the penultimate proline stabilizing the transition state during Fmoc decomposition. The strong basicity of the amine group of the penultimate proline also reduces the energy difference of *cis*- and *trans*-conformers. (*cis*- conformers are more likely to cause self-deprotection and DKP formation.) The intermolecular path-

https://doi.org/10.1021/acsomega.2c05915
ACS Omega 2022, 7, 46809−46824

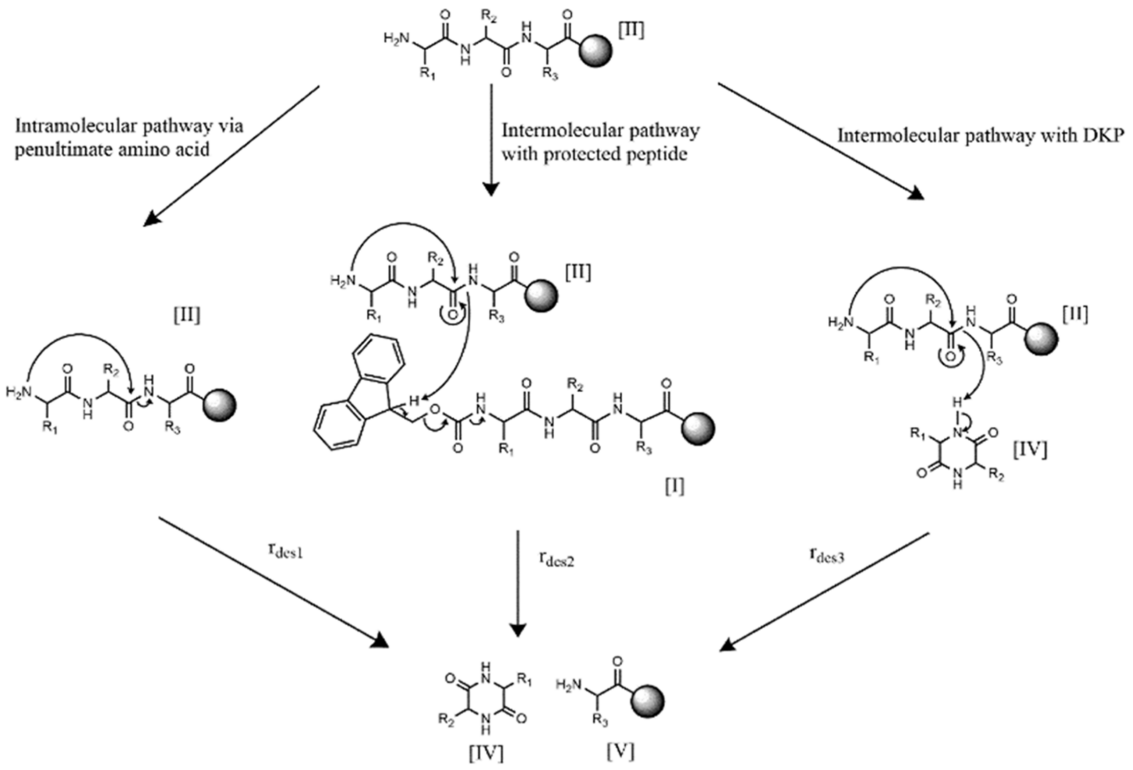

Figure 20. Pseudo-reaction pathways for desXaaXaa formation.

way (ii) becomes significant when the peptide is readily self-deprotected, generating sufficient free $-NH_2$ groups.

The desXaaXaa formation pseudo-reaction pathway is proposed in Figure 20, consisting of three independent pathways: (i) the cyclization reaction pathway triggered by the intramolecular interaction from the amine group of the penultimate amino acid (r_{des1}); (ii) the intermolecular pathway between the amine group of the deprotected peptide and the protected peptide (r_{des2}); (iii) the intermolecular pathway between DKP and the deprotected peptide (r_{des3}). Reaction pathway (i) becomes particularly dominant when proline is the penultimate amino acid. Reaction pathway (ii) was proposed due to the autocatalytic behavior of desXaaXaa formation during the peptide self-deprotection reaction. Reaction pathway (iii) is based on the faster rate of desProPro formation when DKP is added to the H-Pro-Pro-Ser-resin/DMF slurry.

Macro-Kinetics Model. We developed desProPro kinetics equations for self-deprotection (r_{d1} and r_{d2}) and desXaaXaa formation (r_{des1}, r_{des2}, and r_{des3}), which are shown in eqs 1−5. The self-deprotection conversion X and desXaaXaa yield Y can be expressed by eqs 9 and 10.

$$r_{d1} = k_{d1}[\mathrm{I}] \tag{1}$$

$$r_{d2} = k_{d2}[\mathrm{I}]([\mathrm{II}] + [\mathrm{V}])^{0.7} \tag{2}$$

$$r_{des1} = k_{des1}[\mathrm{II}] \tag{3}$$

$$r_{des2} = k_{des2}[\mathrm{I}][\mathrm{II}]^6 \tag{4}$$

$$r_{des3} = k_{des3}[\mathrm{II}][\mathrm{IV}] \tag{5}$$

where [I], [II], and [IV] are the molar fraction of the protected peptide, the deprotected peptide, and DKP. The molar fractions of [I], [II], and [IV] can be expressed using eqs 6−8.

$$[\mathrm{I}] = 1 - X \tag{6}$$

$$[\mathrm{II}] = X - Y \tag{7}$$

$$[\mathrm{IV}] = Y \tag{8}$$

where X represents self-deprotection conversion and Y represents desXaaXaa yield.

$$dX/dt = k_{d1}(1 - X) + k_{d2}(1 - X)X^{0.7} \tag{9}$$

$$dY/dt = k_{des1}(X - Y) + k_{des2}(1 - X)(X - Y)^6 + k_{des3}(X - Y)Y \tag{10}$$

Kinetics parameters are solved using the Matlab optimization toolbox "fminsearch" by minimizing the relative error between simulation and experimental self-deprotection and desXaaXaa data. The kinetics parameters are shown in Supporting Information Table S8. A typical comparison of the model and experiment is presented in Figure 21. As can be seen in Figure 21 and Table 4, the self-deprotection reaction consists of an initial induction stage of pseudo-first-order reaction kinetics dominated by the intramolecular self-deprotection pathway (r_{d1}). Then, self-deprotection proceeds to autocatalytic stage reaction kinetics by the intermolecular self-deprotection pathway (r_{d2}) triggered by the amine group of the deprotected peptide. The desXaaXaa formation reaction mechanism consists of an initial induction stage dominated by the pseudo-first-order reaction of the intramolecular pathway (r_{des1}) triggered by the penultimate amino acid. Then it proceeds into autocatalytic stage I via the desXaaXaa intermolecular pathway (r_{des2}) due to the protected peptide. After all of the protected peptide is consumed, desXaaXaa formation is dominated by autocatalytic stage II, which corresponds to the intermolecular pathway (r_{des3}) via DKP.

https://doi.org/10.1021/acsomega.2c05915
ACS Omega 2022, 7, 46809−46824

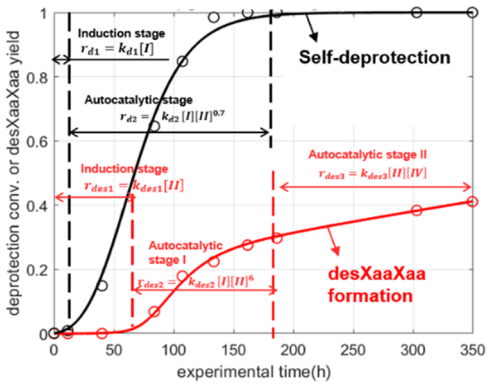

Figure 21. Comparison of experiment (dot marker) and simulation (solid line) results for Fmoc-Gly-Pro-Ser-resin stability in DMF at 20 °C.

The deFmoc and subsequence DKP formation rates are estimated using the macro-kinetics model and the fitting kinetics parameters are presented in Supporting Information Table S8. Comparison between experiments and simulations is shown in Figure S13. As it can be seen, regardless of the peptide sequence, the reaction profiles show similar trends for the distinct phases that are described in Table 4.

CONCLUSIONS

We investigated the root cause of DKP formation during TZP SPPS synthesis and found that a significant amount of desProPro can be formed while holding DMF-wetted Fmoc-Pro-Pro-Ser-resin. This result was highly unexpected as all of the washed Fmoc-protected peptides had been viewed as relatively stable intermediates. Fmoc-Pro-Pro-Ser-resin is also subject to DKP formation during the Fmoc-deprotection reaction with low piperidine equivalent ratios and long deprotection times. These findings are related to the control strategy for TZP where Fmoc-Pro-Pro-Ser-resin is an API intermediate during SPPS. However, when diproline is directly coupled to avoid this intermediate, the DKP formation is not a significant issue since the DKP-sensitive Fmoc-Pro-Pro-Ser-resin is skipped. We found that peptides with penultimate prolines are particularly prone to DKP formation. The reaction mechanism of the penultimate amino acid-driven peptide self-deprotection is proposed, which includes intramolecular pathways between the amine group of the penultimate amino acid and the Fmoc- protecting group and intermolecular pathways between the amine group of the deprotected peptide and the Fmoc group of the protected peptide. Detailed kinetics models were developed for various peptides under different solvents and temperatures, which can be used to predict the API intermediate degradation. At last we proposed the following methods for minimizing the impurities.

- Add oxyma additives (≈0.2 wt %) to the DMF after the coupling reaction or maintain a high residual coupling reagent concentration after post-coupling washes.
- Wash the resin with acetonitrile after the coupling reaction.
- Reduce the hold time and temperature (∼3 °C) after the coupling reaction. We left DMF-wetted Fmoc-Pro37 (after three 5-volume DMF washes post coupling) at 5 °C for 19 h and the deprotection conversion only increased from 0.1 to 1.3%.
- Apply a high piperidine eqv. ratio and short deprotection time.
- Use the Bsmoc-protected amino acid during the coupling reaction for sensitive spots.
- Utilize dimers to bypass DKP-sensitive intermediates.

EXPERIMENTAL SECTION

Chemicals. Fmoc-Gly-OH, Fmoc-Ser(tBu)-OH, Fmoc-Ala-OH, Fmoc-Pro-OH, Sieber amide resin, DMF, piperidine, oxyma, *N*,*N*′-diisopropylcarbodiimide (DIC), trifluoroacetic acid (TFA), and dichloromethane (DCM) were purchased from Sigma Aldrich. The chemicals used did not go through any purification.

Characterization. *Sample Preparation for LC Analysis.* The on-resin peptide sequences evaluated included Fmoc-Pro-Pro-Ser(^{t}Bu)-Resin, Fmoc-Gly-Pro-Ser(^{t}Bu)-Resin, Fmoc-Ala-Pro-Ser(^{t}Bu)-Resin, Fmoc-Pro-Gly-Ser(^{t}Bu)-Resin, and Fmoc-Pro-Ala-Ser(^{t}Bu)-Resin with desXaaXaa impurity after the DKP reaction with H-Ser(^{t}Bu)-OH. The sample preparation steps included collection of 20 mg of resin washed with 10 mL of DMF. Then, 1 mL of activation solution (30 min activation time) was added to the composition of 0.18 M Fmoc-L-Ala-OH, 0.660 M DIC, and 0.750 M Oxyma to allow coupling at 20 °C for 2 h. Then the sample was washed with 10 mL of DMF to remove any residual coupling solution. 1 mL of TFA was added for hard cleavage reaction for 1 h. The sample was diluted with 5 mL of 4:1 v/v DMSO/ACN diluent. The spent resin was filtered and the solution sample was taken for LCMS analysis to check the relative UV response of Fmoc-Ala-Ser-OH. The Fmoc-Ala-Ser-OH was designated as a desProPro impurity (H-Ser(^{t}Bu)-resin after being coupled with Fmoc-Ala-OH) for the desirable Fmoc-Pro-Pro-Ser(^{t}Bu)-resin intermediate. For other peptides with desXaaXaa impurity not being H-Ser(^{t}Bu)-OH, 20 mg of resin was taken and washed thoroughly with 10 mL of DMF and then the hard cleavage reaction was conducted with 1 mL of TFA for 1 h. The sample was then diluted with 5 mL of 4:1 v/v DMSO/ACN diluent for LCMS analysis.

LC−MS Characterization of the Peptide Sample. The chromatographic systems used to analyze the resin samples were from the Agilent 1290 Infinity II line and incorporated a quaternary pump, a vial sampler, and a thermostatted column compartment with an internal 6-port two-position valve, a diode array detector fitted with a 0.6 μL MaxLight flow cell, and an Agilent 6135 MSD single quadrupole mass spectrometer. The column used was a Waters Acquity BEH C8 (150 × 2.1 mm^2, 1.7 μm dp). The mobile phase consisted of 0.1% TFA in water (A) and acetonitrile (B). The flow rate was 0.60 mL/min, column temperature was 65 °C, and

Table 4. Dominant Reaction Pathways in Each Stage

reaction	induction stage (intramolecular)	autocatalytic stage I (intermolecular)	autocatalytic stage II (intermolecular)
self-deprotection	$r_{d1} = k_{d1}[I]$	$r_{d2} = k_{d2}[I][II]^{0.7}$	na
desXaaXaa	$r_{des1} = k_{des1}[II]$	$r_{des2} = k_{des2}[I][II]^6$	$r_{des3} = k_{des3}[II][IV]$

https://doi.org/10.1021/acsomega.2c05915
ACS Omega 2022, 7, 46809−46824

injection volume was 2 μL. A 2 to 75% acetonitrile gradient in 12 minutes was used for elution. UV detection at 40 Hz was done at 214 nm. The mass spectrometer was set to collect the data in full scan mode between 75 and 1500 AMU with a 0.35 s cycle time. The source parameters were +3000 V, with drying gas flow set to 13.0 L/min and drying gas temperature set to 350 °C.

NMR Characterization of DKP and DBF in Solution Phase. ^{1}H NMR (500 MHz, DMF) δ 7.95 (d, J = 7.6 Hz, 2H), 7.90 (d, J = 7.4 Hz, 2H), 7.46 (t, J = 7.4 Hz, 2H), 7.38 (t, J = 7.4 Hz, 2H), 6.33 (s, 2H), 4.34 (t, J = 8.0 Hz, 2H), 3.51 (s, 4H), 3.50−3.38 (m, 2H), 2.37−1.98 (m, 2H), 1.97−1.88 (m, 4H). This represents a mixture of dibenzofulvene (DBF) and a single diastereomer of diketopiperazine (DKP, originating from o) in fully protonated dimethylformamide (DMF).

Computational Details. All computational calculations involved in this study were performed using the Gaussian 16 suite of programs.[33,34] Geometrical structures were optimized with the D3BJ dispersion-corrected B3LYP method with the 6-31G(d) basis set.[35,36] Vibrational frequency calculations were performed on all optimized structures at the same level of theory of geometry optimization. The optimized geometries were verified to be actual minima on the potential energy surface, wherein no negative frequencies were observed. For transition-state (TS) calculations, only one negative frequency was observed. On all the TSs, intrinsic reaction coordinate (IRC) analysis was carried out to confirm the TS connecting the respective reactant and product.[37] *N*,*N*-Dimethylformamide was used as a solvent in the case of Fmoc cleavage; solvent effects were considered with the SMD (solvation model based on density) solvation model.[38] Wavefunction files (.wfn) were generated with Gaussian 16. These.wfn files were used as the input to generate NCI plots with Multiwfn program.[39]

Synthesis Procedures. *Synthesis Condition of Model Peptides.* The solid-phase synthesis of the four model peptides (Figure 14) was executed on the Symphony X synthesizer using an automated program. DMF was used as the solvent for washing, coupling, and deprotection solution makeup. 20% Piperidine/DMF solution was used as the deprotection solution. 0.660 M DIC and 0.750 M Oxyma were used as the activation solution. The amino acids of Fmoc-L-Ala-OH, Fmoc-L-Gly-OH, Fmoc-L-Ser(^{t}Bu)-OH, and Fmoc-L-Pro-OH were prepared at 0.375 M concentration in DMF. The Sieber resin had the loading of 0.76 mmol/g. 0.66 g of each of these resins (0.5 mmol) was taken in 8 reaction vessels (RV). 1 mmol of each of the four peptides was synthesized. The resin was swollen with 2 × 20 mL DMF. Deprotection of the Fmoc was conducted with 4 × 9 mL of 20% v/v piperidine in DMF and 30 min deprotection time. The activation reaction was carried out by mixing 0.18 M 3 equiv of AAs, 3.3 equiv DIC, and 3.0 equiv oxyma for 30 min. Then the coupling was done for 6 h coupling time at 20 °C. After the synthesis, the resins were washed with 5 × 9 mL DCM. They were all dried for 6 h under nitrogen on Symphony X.

Synthesis Condition of the TZP API Intermediates. The TZP intermediates (Table 2 and Figure 8) were sampled from the full synthetic builds of TZP API. The full builds were conducted in 6 L jacketed filter reactors using an in-house automation system. The builds were done on Sieber resin with a loading of 0.75 mmol/g. DMF was used as the solvent for all steps of the process. The Fmoc deprotection was achieved using 20 vol % piperidine in DMF. The solutions of amino acids, oxyma, and DIC were prepared in DMF. Solutions were prepared with the desired mmol/g concentration, which allowed for the mass-based feed system to deliver the molar target without needing solution density. Each build started with 100 mmol of Sieber resin and all steps were conducted at 25 °C, apart from the amino acid activation done at 20 °C. The syntheses started by swelling the resin twice with 9 mL DMF/g of the initial resin charge (the initial resin mass charge was the basis for all charge volumes; in this case 9 mL/g resin, or 9 V, is 1200 mL). The Fmoc deprotection was achieved using three or four 9 V charges of piperidine. Each deprotection charge was stirred for 30 min. After deprotection, the reactor bed was washed with consecutive 9 V DMF charges and stirred for 5 min until the residual piperidine in the reactor effluent was not more than 600 ppm. This required between 5 and 7 washes. Activation of the amino acid to the activated ester was accomplished in a separate reactor, where the target amino acid, Oxyma, and DIC, along with pure DMF to adjust the volume, were added together in the necessary proportions to achieve a volume of 7.25 V and 2.5 molar equivalents of amino acid, 2.5 molar equivalents of Oxyma, and 2.75 molar equivalents of DIC. The activation reaction was stirred for 30 min at 20 °C, then transferred to the filter reactor for coupling at 25 °C. Most couplings were stirred for 4 h before sampling to confirm the reaction completion. The exceptions were 6 h coupling times for Pro38, Pro37, and Pro36, as well as an 8 h coupling for Lys20, due to the bulky ivDde-protecting group. After coupling, the activation reactor and the resin bed were washed with DMF. The first three washes were fed in series from the activation reactor to the resin bed, while the final two washes were fed directly to the resin bed. Each wash contained 9 volumes of DMF and stirred for 5 min. During the syntheses of the full TZP molecule, large samples were taken and saved. The reduction in reactor contents was calculated and the subsequent charge quantities were reduced proportionally. These large samples were the source of the TZP intermediates tested as part of this wok.

■ ASSOCIATED CONTENT

Supporting Information

The Supporting Information is available free of charge at https://pubs.acs.org/doi/10.1021/acsomega.2c05915.

Impact of temperature; deprotection conditions; oxyma addition; solvent composition; DKP/DBF additive, and protection group on the self-deprotection and double amino acid deletion impurity formation (PDF)

■ AUTHOR INFORMATION

Corresponding Authors

Jingyao Wang − *Synthetic Molecule Design and Development, Eli Lilly and Company, Indianapolis, Indiana 46285, United States*; Email: wang_jingyao@lilly.com

Michael E. Kopach − *Synthetic Molecule Design and Development, Eli Lilly and Company, Indianapolis, Indiana 46285, United States*; orcid.org/0000-0002-3590-702X; Email: kopach_michael@lilly.com

Authors

Mark R. Berglund − *Synthetic Molecule Design and Development, Eli Lilly and Company, Indianapolis, Indiana 46285, United States*

https://doi.org/10.1021/acsomega.2c05915
ACS Omega 2022, 7, 46809−46824

Timothy Braden − *Synthetic Molecule Design and Development, Eli Lilly and Company, Indianapolis, Indiana 46285, United States*

Matthew C. Embry − *Synthetic Molecule Design and Development, Eli Lilly and Company, Indianapolis, Indiana 46285, United States*

Martin D. Johnson − *Synthetic Molecule Design and Development, Eli Lilly and Company, Indianapolis, Indiana 46285, United States;* orcid.org/0000-0003-1260-7478

Stephen R. Groskreutz − *Synthetic Molecule Design and Development, Eli Lilly and Company, Indianapolis, Indiana 46285, United States*

Fareed Bhasha Sayyed − *Synthetic Molecule Design & Development, Eli Lilly Services India Pvt. Ltd., Bengaluru 560103, India;* orcid.org/0000-0001-8364-4810

Sergey Vladimirovich Tsukanov − *Synthetic Molecule Design and Development, Eli Lilly and Company, Indianapolis, Indiana 46285, United States;* orcid.org/0000-0003-4287-7268

Timothy D. White − *Synthetic Molecule Design and Development, Eli Lilly and Company, Indianapolis, Indiana 46285, United States*

Ankur Jalan − *Synthetic Molecule Design and Development, Eli Lilly and Company, Indianapolis, Indiana 46285, United States*

Kevin D. Seibert − *Synthetic Molecule Design and Development, Eli Lilly and Company, Indianapolis, Indiana 46285, United States*

Complete contact information is available at: https://pubs.acs.org/10.1021/acsomega.2c05915

Author Contributions

The manuscript was written through the contributions of all authors. All authors have given approval to the final version of the manuscript.

Notes

The authors declare no competing financial interest.

■ ACKNOWLEDGMENTS

The authors thank S. O'Keeffe, C. Cruz, S. Langan, D. Mergott, S. Ryan, S. Kolis, J. Howell, and W. Roth for the management support of these efforts. The authors acknowledge Dr. Yu Lu for technical consultation discussion.

■ REFERENCES

(1) Frederick, M. O.; Boyse, R. A.; Braden, T. M.; Calvin, J. R.; Campbell, B. M.; Changi, S. M.; Coffin, S. R.; Condon, C.; Gowran, O.; Groh, J. M.; Groskreutz, S. R.; Harms, Z. D.; Humenik, A. A.; Kallman, N. J.; Klitzing, N. D.; Kopach, M. E.; Kretsinger, J. K.; Lambertus, G. R.; Lampert, J. T.; Maguire, L. M.; Moynihan, H. A.; Mullane, N. S.; Murphy, J. D.; O'Mahony, M. E.; Richey, R. N.; Seibert, K. D.; Spencer, R. D.; Strege, M. A.; Tandogan, N.; Torres, F. L. T.; Tsukanov, S. V.; Xia, H. Kilogram-Scale GMP Manufacture of Tirzepatide Using a Hybrid SPPS/LPPS Approach with Continuous Manufacturing. *Org. Process Res. Dev.* **2021**, *25*, 1628−1636.

(2) Johnson, M. D.; Kopach, M. E.; Webster, L. P.Three resin reactors in series peptide synthesizerWO 202115844 A2, 2021-08-12.

(3) Brunfeldt, K.; Christensen, T.; Roepstorff, P. Acetylation an artefact in solid phase peptide synthesis. A mass spectrometrical investigation. *FEBS Lett.* **1972**, *25*, 184−188.

(4) Gairí, M.; Lloyd-Williams, P.; Albericio, F.; Giralt, E. Use of BOP reagent for the suppression of diketopiperazine formation in boc/bzl solid-phase peptide synthesis. *Tetrahedron Lett.* **1990**, *31*, 7363−7366.

(5) Pawlas, J.; Nuijens, T.; Persson, J.; Svensson, T.; Schmidt, M.; Toplak, A.; Nilsson, M.; Rasmussen, J. H. Sustainable, cost-efficient manufacturing of therapeutic peptides using chemo-enzymatic peptide synthesis (CEPS). *Green Chem.* **2019**, *21*, 6451−6467.

(6) Khosla, M. C.; Smeby, R.; Bumpus, F. Failure sequence in solid-phase peptide synthesis due to the presence of an N-alkylamino acid. *J. Am. Chem. Soc.* **1972**, *94*, 4721−4724.

(7) Rothe, M.; Mazánek, J. Side-reactions arising on formation of cyclodipeptides in solid-phase peptide synthesis. *Angew. Chem., Int. Ed.* **1972**, *11*, 293.

(8) Martinez, J.; Bodanszky, M. SIDE REACTIONS IN PEPTIDE SYNTHESIS: IX.* Suppression of the Formation of Aminosuccinyl Peptides with Additives. *Int. J. Pept. Protein Res.* **1978**, *12*, 277−283.

(9) Rydon, H. N.; Smith, P. 702. Polypeptides. Part IV. The self-condensation of the esters of some peptides of glycine and proline. *J. Am. Chem. Soc.* **1956**, 3642−3650.

(10) D'Hondt, M.; Bracke, N.; Taevernier, L.; Gevaert, B.; Verbeke, F.; Wynendaele, E.; De Spiegeleer, B. Related impurities in peptide medicines. *J. Pharm. Biomed. Anal.* **2014**, *101*, 2−30.

(11) Gisin, B. F.; Merrifield, R. Carboxyl-catalyzed intramolecular aminolysis. Side reaction in solid-phase peptide synthesis. *J. Am. Chem. Soc.* **1972**, *94*, 3102−3106.

(12) Petersen, R.; Le Quement, S. T.; Nielsen, T. E.; Solid-phase iminium cyclization reactions for the synthesis of natural product-like diketopiperazines. (2013) ABSTRACTS OF PAPERS OF THE AMERICAN CHEMICAL SOCIETY, Volume 245 [829-ORGN].

(13) Sun, X.; Rai, R.; MacKerell, A. D., Jr.; Faden, A. I.; Xue, F. Facile one-step synthesis of 2, 5-diketopiperazines. *Tetrahedron Lett.* **2014**, *55*, 1905−1908.

(14) Suzuki, K.; Nitta, K.; Endo, N. Suppression of diketopiperazine formation in solid phase peptide synthesis. *Chem. Pharm. Bull.* **1975**, *23*, 222−224.

(15) Yang, Y.; Hansen, L. Optimized Fmoc-Removal Strategy to Suppress the Traceless and Conventional Diketopiperazine Formation in Solid-Phase Peptide Synthesis. *ACS Omega* **2022**, *7*, 12015−12020.

(16) Pedroso, E.; Grandas, A.; de las Heras, X.; Eritja, R.; Giralt, E. Diketopiperazine formation in solid phase peptide synthesis using p-alkoxybenzyl ester resins and Fmoc-amino acids. *Tetrahedron Lett.* **1986**, *27*, 743−746.

(17) Goolcharran, C.; Borchardt, R. T. Kinetics of diketopiperazine formation using model peptides. *J. Pharm. Sci.* **1998**, *87*, 283−288.

(18) Jadhav, S.; Martin, V.; Egelund, P. H.; Castro, H. J.; Krüger, T.; Richner, F.; Le Quement, S. T.; Albericio, F.; Dettner, F.; Lechner, C.; et al. Replacing DMF in solid-phase peptide synthesis: varying the composition of green binary solvent mixtures as a tool to mitigate common side-reactions. *Green Chem.* **2021**, *23*, 3312−3321.

(19) Alsina, J.; Giralt, E.; Albericio, F. Use of N-tritylamino acids and PyAOP1 for the suppression of diketopiperazine formation in Fmoc/tBu solid-phase peptide synthesis using alkoxybenzyl ester anchoring linkages. *Tetrahedron Lett.* **1996**, *37*, 4195−4198.

(20) Fischer, P. M. Diketopiperazines in peptide and combinatorial chemistry. *J. Pept. Sci.* **2003**, *9*, 9−35.

(21) Coin, I.; Dölling, R.; Krause, E.; Bienert, M.; Beyermann, M.; Sferdean, C. D.; Carpino, L. A. Depsipeptide methodology for solid-phase peptide synthesis: circumventing side reactions and development of an automated technique via depsidipeptide units. *J. Org. Chem.* **2006**, *71*, 6171−6177.

(22) Coin, I.; Beyermann, M.; Bienert, M. Solid-phase peptide synthesis: from standard procedures to the synthesis of difficult sequences. *Nat. Protoc.* **2007**, *2*, 3247−3256.

(23) Nishio, M. CH/π hydrogen bonds in crystals. *CrystEngComm* **2004**, *6*, 130−158.

(24) Ganguly, H. K.; Majumder, B.; Chattopadhyay, S.; Chakrabarti, P.; Basu, G. Direct evidence for CH··· π interaction mediated stabilization of pro-cis pro bond in peptides with pro-pro-aromatic motifs. *J. Am. Chem. Soc.* **2012**, *134*, 4661−4669.

(25) Seguin, T. J.; Lu, T.; Wheeler, S. E. Enantioselectivity in catalytic asymmetric fischer indolizations hinges on the competition of π-stacking and CH/π interactions. *Org. Lett.* **2015**, *17*, 3066−3069.

(26) Platzer, G.; Mayer, M.; Beier, A.; Brüschweiler, S.; Fuchs, J. E.; Engelhardt, H.; Geist, L.; Bader, G.; Schörghuber, J.; Lichtenecker, R. PI by NMR: probing CH−π interactions in protein−ligand complexes by NMR spectroscopy. *Angew. Chem.* **2020**, *132*, 14971−14978.
(27) Johnson, E. R.; Keinan, S.; Mori-Sánchez, P.; Contreras-García, J.; Cohen, A. J.; Yang, W. Revealing noncovalent interactions. *J. Am. Chem. Soc.* **2010**, *132*, 6498−6506.
(28) Wang, J.; Sun, Y.; Gao, X.; Mannan, M. S.; Wilhite, B. Experimental study of electrostatic hazard inside scrubber column using response surface methodology. *Chem. Eng. Sci.* **2019**, *200*, 46−68.
(29) Wang, J.; Mannan, M. S.; Wilhite, B. A. Integrated thermodynamic and kinetic model of homogeneous catalytic N-oxidation processes. *AlChE J.* **2020**, *66*, No. e16875.
(30) Wang, J.; Huang, Y.; Wilhite, B. A.; Papadaki, M.; Mannan, M. S. Toward the identification of intensified reaction conditions using response surface methodology: a case study on 3-methylpyridine N-oxide synthesis. *Ind. Eng. Chem. Res.* **2019**, *58*, 6093−6104.
(31) Lin, Z.; Wang, J.; Nikolakis, V.; Ierapetritou, M. Process flowsheet optimization of chemicals production from biomass derived glucose solutions. *Comput. Chem. Eng.* **2017**, *102*, 258−267.
(32) Sun, Y.; Wang, J.; Zhu, W.; Yuan, S.; Hong, Y.; Mannan, M. S.; Wilhite, B. Development of consequent models for three categories of fire through artificial neural networks. *Ind. Eng. Chem. Res.* **2020**, *59*, 464−474.
(33) Frisch, M.; Trucks, G.; Schlegel, H.; Scuseria, G.; Robb, M.; Cheeseman, J.; Scalmani, G.; Barone, V.; Petersson, G.; Nakatsuji, H.*Gaussian 16*; Gaussian Inc.: Wallingford CT, 2016.
(34) Xia, R.; Wang, J.; Han, Z.; Li, Z.; Mannan, M. S.; Wilhite, B. Mechanism study of ammonium nitrate decomposition with chloride impurity using experimental and molecular simulation approach. *J. Hazard. Mater.* **2019**, *378*, No. 120585.
(35) Becke, A. D. Density-functional thermochemistry. I. The effect of the exchange-only gradient correction. *J. Chem. Phys.* **1992**, *96*, 2155−2160.
(36) Grimme, S.; Ehrlich, S.; Goerigk, L. Effect of the damping function in dispersion corrected density functional theory. *J. Comput. Chem.* **2011**, *32*, 1456−1465.
(37) Fukui, K. The path of chemical reactions-the IRC approach. *Acc. Chem. Res.* **1981**, *14*, 363−368.
(38) Marenich, A. V.; Cramer, C. J.; Truhlar, D. G. Universal solvation model based on solute electron density and on a continuum model of the solvent defined by the bulk dielectric constant and atomic surface tensions. *J. Phys. Chem. B* **2009**, *113*, 6378−6396.
(39) Lu, T.; Chen, F. Multiwfn: a multifunctional wavefunction analyzer. *J. Comput. Chem.* **2012**, *33*, 580−592.

https://doi.org/10.1021/acsomega.2c05915
ACS Omega 2022, 7, 46809−46824